ORIGINAL ARTICLE

Potential of cold-atom airborne gravimetry to improve coastal gravity field and quasigeoid modelling

Dinh Toan Vu[1,2] · Sylvain Bonvalot[1] · Lucia Seoane[1] · Germinal Gabalda[1] · Dominique Remy[1] · Sean Bruinsma[1,3] · Yannick Bidel[4] · Alexandre Bresson[4] · Nassim Zahzam[4] · Didier Rouxel[5] · Corinne Salaün[5] · Marie-Françoise Lalancette[5] · René Forsberg[6] · Tim Jensen[6] · Olivier Jamet[7,8]

Abstract

We investigate using the GIRAFE cold-atom gravimeter during an airborne gravity survey for improving gravity field and quasigeoid modelling. The study is conducted over the Bay of Biscay, France. Geoid/quasigeoid determination is usually a major challenge over such coastal areas due to scarce and inconsistent gravity data. In a first step, the GIRAFE dataset is analysed and compared with available surface gravity data as well as with global altimetry models from UCSD and DTU. The comparisons indicate that the DTU model is better than the UCSD model within around 10 km from the coastline. Furthermore, recent satellite altimeter missions significantly improve the altimetry models in coastal areas. A significant bias (− 4.00 mGal) in shipborne data is also found from this comparison. In a second step, eight quasigeoid solutions are calculated to evaluate the contribution of GIRAFE data. This contribution reaches 3 cm in terms of height anomaly for DTU21 while being much larger for UCSDv31 and shipborne data. Finally, the quasigeoid solutions are validated using GNSS-levelling data. The results indicate that using GIRAFE data improves by approximately 50% the quality of quasigeoid models over land near the coast. The highest accuracy, around 1 cm, is achieved when GIRAFE data are merged with refined gravity data. Importantly, the standard deviation is just 1.2 cm when compared with GNSS-levelling points if using only GIRAFE data over marine areas, which is very close to the 1 cm goal of geoid/quasigeoid model determination in modern geodesy. This study thus confirms the benefits of performing airborne gravity survey using quantum sensors.

Keywords Absolute airborne gravity · Quantum gravimeter · Satellite altimetry · Shipborne gravity · Quasigeoid · GNSS-levelling

✉ Dinh Toan Vu
   dinhtoan.vu@get.omp.eu

1   Géosciences Environnement Toulouse (GET), CNRS, CNES, IRD, UT3, Université de Toulouse, 31400 Toulouse, France

2   Department of Geodesy, Hanoi University of Mining and Geology, Hanoi 10000, Vietnam

3   Centre National D'Etudes Spatiales (CNES), 18 avenue Edouard Belin, 31400 Toulouse, France

4   DPHY, ONERA, Université Paris Saclay, 91123 Palaiseau, France

5   SHOM, French Hydrographic and Oceanographic Office, CS 92803, 29228 Brest, France

6   National Space Institute, Technical University of Denmark, Kongens Lyngby, Denmark

7   Institut de Physique du globe de Paris, Université de Paris, CNRS, IGN, 75005 Paris, France

8   ENSG-Géomatique, IGN, 77455 Marne-la-Vallée, France

1 Introduction

Coastal gravity field and geoid/quasigeoid models play a crucial role in oceanography, geodesy and geophysics. They are used for studying coastal ocean dynamic topography and currents (Ophaug et al. 2015; Forsberg et al. 2017), sea level change (Huang 2017), GNSS-levelling and height system unification (Vu et al. 2020) and Earth's interior (Hipkin 2000; Vu et al. 2021a). Global offshore gravity models inferred from satellite altimetry data map the gravity field over sea in a very homogeneous way. The spatial resolution of these global altimetric models is limited mainly due to measurement cadence and ground track spacing. It is well-known that the accuracy and spatial resolution of these models are reduced close to the coast (Andersen 1999; Andersen and

Knudsen 2000). The main reasons for this are back-scattering from land points, loss of signal track on the sea surface near to the coast and poorer accuracy of the applied corrections to the altimeter data (Andersen and Scharroo 2011). Shipborne gravimeters can measure gravity with high resolution, but the spatial distribution is often inhomogeneous and limited due to difficult conditions, such as shallow water regions near the coast (Olesen et al. 2002). The severe lack of gravity data remains a barrier for studies in coastal areas. Moreover, heterogeneous gravity observations on open sea, in coastal zones, and over land suffer from inconsistencies in terms of spatial resolutions and accuracies (Hirt 2013), which makes their combination difficult. Thanks to the development of GNSS in the early 1990s, airborne gravimetry can be routinely carried out not only for research but also for resource investigation (Brozena 1992). Regional gravity field and gravimetric geoid/quasigeoid models can be developed on the basis of this technique. The data gaps of traditional gravimetry on land and altimetry-derived gravity fields and/or shipborne gravimetry techniques on sea can be filled by airborne gravity measurements (Forsberg and Olesen 2010). These airborne measurements provide a seamless coverage over both sea and land with uniform accuracy, making them particularly valuable in the modelling of coastal gravity fields and gravimetric geoids/quasigeoids (Wu et al. 2019).

In the last two decades, gravimetry campaigns on aircraft were carried out in several countries/regions to complete, modernize as well as update national gravity field databases (e.g. France-Switzerland (Verdun et al. 2003), Taiwan (Hwang et al. 2007), Mongolia (Forsberg et al. 2007), USA GRAV-D project (Smith et al. 2013), Nepal (Forsberg et al. 2014), New Zealand (McCubbine et al. 2018) and Philippines (Gatchalian et al. 2022)). All these campaigns were performed with relative gravimeters requiring regular calibration, which imposes significant constraints (Bidel et al. 2020). An absolute cold-atom gravimeter called GIRAFE was developed and tested successfully on ship (Bidel et al. 2018) and aircraft (Bidel et al. 2020, 2023). In these test campaigns, the GIRAFE absolute gravimeter has been compared with classical gravimeters. The precision of the GIRAFE is equal to or better than that of classical instruments. Moreover, through validation with the available surface data it has been shown that the accuracy of the GIRAFE gravity data is 1–1.5 mGal, showing the great potential of the instrument. However, the impact of the GIRAFE gravity data on the determination of a high-resolution and high-accuracy geoid/quasigeoid model was so far never assessed.

The accuracy of altimetric gravity field models was substantially improved thanks to recent satellite altimeter missions (Sandwell et al. 2014; Verron et al. 2015; Andersen and Knudsen 2020). The new generation of satellite altimeter missions, especially those with Synthetic Aperture Radar—SAR and SAR Interferometric—SARIn modes, e.g. CryoSat-2 and Sentinel-3 (Abulaitijiang et al. 2015; Bonnefond et al. 2018), or with Ka-band of the SARAL/AltiKa mission (Verron et al. 2021), allows reliable gravity data to be acquired closer to coast (Green et al. 2019). Consequently, the recent altimetric gravity field models may be significantly improved in the coastal areas. But this needs to be validated. In this study, the improvement of the latest altimetric models will be validated and quantified by comparison with the GIRAFE airborne gravity data.

Airborne gravity measurements have been employed to estimate regional geoid/quasigeoid models in a number of studies, including coastal regions (Kearsley et al. 1998; Hwang et al. 2006; Bastos et al. 2000; McCubbine et al. 2018; Wu et al. 2019) and mountainous regions (Forsberg et al. 2014; Jiang 2018; Hwang et al. 2020; Varga et al. 2021; Grigoriadis et al. 2021). All these studies highlighted the great potential of the airborne gravity data for more accurate gravity field and gravimetric geoid/quasigeoid models. However, the lack of control data resulting from the difficulties of access for gravity, GNSS and levelling surveys is the main problem for validating the contribution of airborne data (McCubbine et al. 2018; Wu et al. 2019; Grigoriadis et al. 2021). Moreover, the surface and/or satellite gravity data may also significantly reduce the contribution of airborne gravity data because of the lower quality of altimetric data and/or the bias of relative shipborne gravity data in coastal zones. So, the data should be carefully processed and validated before combining them. Here, we use the GIRAFE absolute airborne gravity data to validate the surface and satellite altimeter-derived gravity data. So far the goal of 1 cm geoid accuracy has not been reached, not even when combining ground gravity data with airborne gravity data (Wang et al. 2021), as attempted in the Colorado experiment by 14 groups. It should be noted that this is a mountainous region with heights up to 3000 m where complex topographic effects make it difficult to process airborne gravity data. A highly accurate regional geoid/quasigeoid model is therefore still a challenge.

The main aim of our research is to explore the great potential of new absolute data recently acquired with the GIRAFE quantum gravimeter (Bidel et al. 2023) for: (i) assessing shipborne gravity data in the surveyed area, (ii) quantifying and calibrating/validating locally recent satellite altimeter-derived gravity models and (iii) improving the accuracy in the modelling of the local/regional gravity field and quasigeoid in a coastal study area. As both terrestrial gravity and GNSS-levelling data have good spatial coverage in the onshore zone of the study area, this region is likely to make the assessment of the contribution of airborne gravity data in determining a coastal quasigeoid model possible. In the next section, the study region and available data are presented. In Sect. 3, the methodology used for determining quasigeoid is described.

Section 4 presents the processing and validation results of the available gravity data. In Sect. 5, the results of the gravimetric quasigeoid determination are presented and discussed. Finally, conclusions are drawn and perspectives are given on the contribution of GIRAFE airborne gravity data.

2 Study region and data

The research region is situated on the Bay of Biscay along the western coast of France, where a GIRAFE absolute airborne gravity survey took place on April 23 and 24, 2019 (Bidel et al. 2023). This area (see Fig. 1) was surveyed to prove the ability to homogeneously map gravity fields over sea–land transitions. Shipborne and ground gravity data are additionally available in the study region. Recently released global altimetric gravity field models are also used in this research. First, the airborne gravity estimates will be used to compare with the available gravity data in the study region. Then, different gravity data combination strategies will be presented to estimate the regional quasigeoid. Finally, a high-quality local GNSS-levelling dataset will be used to evaluate the effect of airborne gravity in combination with ground and marine gravity data. The red rectangle in Fig. 1a represents the region for which the gravimetric quasigeoid model is computed, $44° \leq \varphi \leq 45°$ and $-3° \leq \lambda \leq -0.5°$.

2.1 Airborne gravity measurement

The airborne gravity survey of the Bay of Biscay contained six west–east oriented traverse lines spaced at 10 km, and five north–south direction tie lines spaced at 20 km (Fig. 1b). The aircraft flew at an altitude of 1.5 km above the mean sea level, and the average velocity was about 100 m/s.

The details of the data processing of the cold-atom gravimeter observations and GNSS data were presented in Bidel et al. (2020, 2023). A Gaussian low-pass filter is used for noise reduction in the GIRAFE gravity measurements. The 70 s low-pass filter gave the best fit with marine gravity (Bidel et al. 2023) and will be used thereafter. The airborne gravity data include geodetic longitude (λ), geodetic latitude (φ), GNSS-derived ellipsoidal height (h) and gravity value (g). The free-air gravity anomaly is then obtained as follows (Hofmann-Wellenhof and Moritz 2006):

$$\Delta g_{\mathrm{FA}} = g - \gamma \tag{1}$$

where γ was calculated from:

$$\gamma = \gamma_0 \left[1 - 2\left(1 + f + m - 2f\sin^2\varphi\right)\frac{H^*}{\alpha} + 3\left(\frac{H^*}{\alpha}\right)^2 \right] \tag{2}$$

where γ_0 denotes the normal gravity value on the reference ellipsoid, GRS80 in this study. This gravity value is determined by Somigliana's rigorous formula (Eq. 2–146 in Hofmann-Wellenhof and Moritz 2006), m denotes the ratio of centrifugal force and gravity at the equator (Eq. 2–180 in Hofmann-Wellenhof and Moritz 2006), f denotes the geometrical flattening of the GRS80 ellipsoid, φ denotes the geodetic latitude, H^* expresses the normal height and α denotes the equatorial radius.

To compute the free-air airborne gravity anomalies, the GNSS geometric heights were converted to normal heights using EGM2008-derived height anomalies (Pavlis et al. 2012). However, the height system of France, NGF-IGN69, is the reference for calculating gravity anomalies in France. In this study, the height anomalies are computed with EGM2008 using a conventional reference geopotential (W_0) (Sánchez et al. 2016), whereas the NGF-IGN69 refers to national mean sea level (Marseille tide gauge station). We used all co-located GNSS-levelling data over France to determine the vertical datum offset (VDO) of the NGF-IGN69 to the equipotential surface defined by the conventional value W_0 = 62,636,853.4 $\mathrm{m^2 s^{-2}}$ (the local GNSS-levelling data in France will be described in Sect. 2.4), which is estimated at 0.87 m. This VDO value is applied to fit EGM2008 to the NGF-IGN69. This step is to avoid inconsistency in the height data related to the gravity data on land/ship and the airborne gravity data.

The estimated error of the gravity disturbance differences at the intersection points between traverse and tie lines of GIRAFE data in the Bay of Biscay was estimated at 1.32 mGal in Bidel et al. (2023). In this campaign, two classical relative gravimeters, LaCoste and Romberg (L&R) S-type (serial number S-38) (Valliant 1992) and iMAR strapdown (Jensen et al. 2019), were also installed on board the aircraft to compare with GIRAFE. The comparison shows that the difference in gravity disturbance between GIRAFE with iMAR and L&R observations has standard deviation (SD) of 2.47 and 7.5 mGal, respectively. Similar precision at crossover points has been achieved for the GIRAFE and iMAR gravimeters, with estimated errors of 1.32 and 1.33 mGal, respectively. The L&R gravimeter provides much less precise gravity measurements due to the L&R platform's inability to properly attenuate the dynamic environment of the aircraft. The variations in roll and pitch angles were significant. Secondly, the upward continued land gravity disturbance in combination with shipborne or satellite altimeter-derived gravity data was compared with the GIRAFE gravity disturbance data at the aircraft's altitude. The SD of these differences is 2.17 and 1.93 mGal, respectively. With the iMAR, the SD is 3.23 and 2.78 mGal, respectively. The SD is again larger for the L&R (8.09 and 7.48 mGal, respectively). This demonstrates the potential of GIRAFE as an absolute airborne gravimeter. Airborne
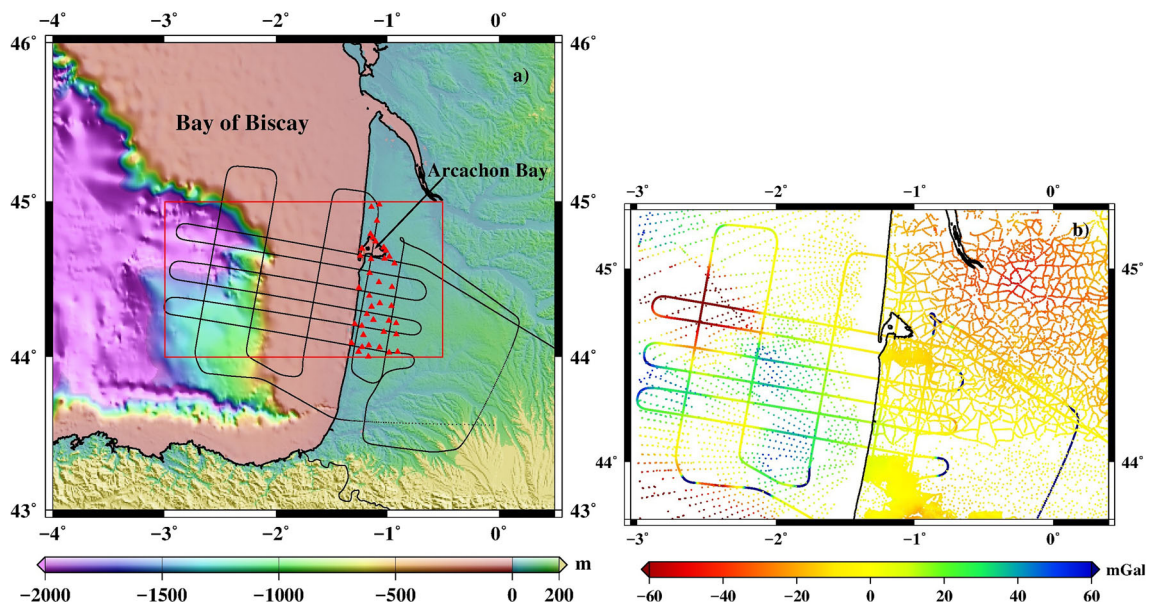
Fig. 1 a Terrain and bathymetry around the Bay of Biscay. The SRTM3arc_v4.1 with resolution of 3″ (Farr et al. 2007) and the SRTM15arc_plus with resolution of 15" (Tozer et al. 2019) were used over land and sea, respectively. Black dots are the airborne gravity data. Red triangles are the local GNSS-levelling data. **b** Distribution of ground and shipborne gravity anomalies and GIRAFE data at the aircraft's altitude in the study region

gravity anomalies must be downward continued from the aircraft's altitude to the Earth's surface, which will be presented in Sect. 4.

2.2 Land and shipborne gravity data

A total number of 17,686 land and 2101 shipborne gravity measurements available from the BGI (Bureau Gravimétrique International) database (see terms of references in Bonvalot (2020)) were used in this study. Details of data sources and surveys are given in section "Data Availability Statement". The accuracy of land and shipborne gravity data (hereafter referred to as surface gravity data) from the BGI database is estimated to be 1 and 2 mGal, respectively. These values were used as uncertainties on surface gravity observations in this study. The gravity data include geodetic longitude (λ), geodetic latitude ('), normal height (H^*) in the NGF-IGN69 reference and the gravity value (g) given in the IGSN71 gravity reference system. In this study, we use Molodensky's theory (Molodensky 1962) to determine a gravimetric quasigeoid model. Therefore, the free-air gravity anomalies computed on the Earth's surface are used in the present study. This gravity anomaly is determined by the difference between the measured gravity value on the Earth's surface (g) and the normal gravity at the associated normal height (γ). We use Eqs. (1) and (2) to determine the free-air surface gravity anomaly.

Figure 1b shows the spatial distribution of gravity data on land and sea. The main challenge when using shipborne gravity data, in particular the older datasets, is that they can be biased due to drift in relative sensors and incorrect positioning (Wessel and Watts 1988). Although crossover analysis between ship tracks and/or comparison with altimetric gravity field models has been applied to reduce this drift, the absolute bias remains. This complicates and on occasion precludes the use of these gravity data for geodetic, geophysical or geological applications or interpretations. Consequently, independent high-resolution gravity data are generally required to detect and completely eliminate the bias in ship gravity data. We used the absolute airborne gravity data to estimate this bias. The coastal zone of our study region (~ 10 km from the coastline) is almost inaccessible for gravity survey by ship. This is an opportunity to evaluate the possible contribution of airborne gravimetry to the mapping of the un-surveyed strip between the available land gravity data and the marine gravity data.

The surface gravity data employed in the present study are consistent with those used in the determination of the recent French gravimetric quasigeoid 2016 (QGF16) (L'Écu 2017), as well as with EGM2008. The GIRAFE airborne gravity data were not employed in either model. Hence, the improvement of the calculated gravimetric quasigeoid model, if any, when compared with the QGF16 and EGM2008 also represents the contribution of GIRAFE data.

Table 1 Recent satellite altimetry-derived gravity field models

N°	Models	Year	Data
1	UCSDv25	2017	ERS-1, Geosat, Cryosat-2/LRM data for one year and Cryosat-2/SAR data for more than two years were added and one year of SARAL/AltiKa
2	UCSDv27	2019	Re-tracked Jason-2 data for one year and SARAL/AltiKa for two months were added
3	UCSDv29	2019	Sentinel-3A/B data for two years were added
4	UCSDv31	2021	SARAL/AltiKa, Cryosat-2/LRM, Cryosat-2 SAR and Sentinel-3A/B for nine months were added
5	DTU15	2015	Re-tracked ERS-1, Geosat, Jason-1 and Cryosat-2
6	DTU17	2017	One year of Cryosat-2, 406 days of Jason-1 and one year of SARAL/AltiKa were added
7	DTU21	2021	Sentinel-3A for five years and Sentinel-3B for three years were added and reprocessed Cryosat-2

2.3 Satellite altimeter-derived gravity data

The latest released satellite altimeter-derived gravity field models, which were computed by the DTU (Technical University of Denmark), called DTU series models (Andersen and Knudsen 1998) and the Scripps Institution of Oceanography—SIO (University of California San Diego-UCSD), called UCSD series models (Sandwell and Smith 1997), are used in this study. Thanks to new altimeter data, these recent models have substantially improved accuracy compared with the older models (Sandwell et al. 2014; Andersen and Knudsen 2020). However, the problem of accuracy near the coast still exists. Specifically, the gravity fields derived from the altimeter data can generally reach an accuracy of a few mGal over open oceans. However, this accuracy may be reduced to tens of mGal over coastal areas (Sandwell et al. 2014). The DTU and UCSD series models employ different types of estimation algorithms. The residual sea surface heights (SSHs) are used by DTU, whereas the residual slopes of the SSH are employed by UCSD. The method of DTU results in higher accuracy in coastal areas, whereas UCSD models are preferred in open sea (Pavlis et al. 2012). Thanks to high-quality GIRAFE data, we can exactly quantify which model is more accurate for the study area. The satellite altimetry-derived gravity field models used in this study are listed in Table 1. The EGM2008-derived gravity anomaly data were spline interpolated onto a 1 min grid and used in both the DTU (Andersen and Knudsen 2020) and UCSD series models to complete land coverage (Sandwell et al. 2014).

2.4 GNSS-levelling data

From 2008 to 2020, the levelling network was revisited within the ERNIT project (French maintenance of levelling network using triplets) by the Institut National de l'Information Géographique et Forestière-IGN. As an important part of this work, IGN performed 3D GNSS positioning on a set of 12,629 levelled points well distributed throughout the country (1 point/40 km^2). The GNSS observations were carried out using dual-frequency receivers and choke ring antennas with a minimum measurement time of 2.5 h per site. The GNSS data in France were processed by IGN using the Bernese scientific software to obtain GRS80-ellipsoidal heights. The ellipsoidal heights were determined with an accuracy of about 2–3 cm. The national height system of France (NGF-IGN69) was rehabilitated by IGN from 1962 to 1969, but the fundamental point was retained. The zero-level of NGF-IGN69 was determined following observations made by the Marseille tide gauge station from 1 February 1885 to 1 January 1897. Normal height is currently used in France. Its levelling network allows misclosure of $2\sqrt{D}$–$5\sqrt{D}$ mm, where D is the distance in km along the levelling line. The local GNSS-levelling data include geodetic longitude (λ), geodetic latitude ('), GRS80-geometric heights (h) and normal heights (H^*). We use this GNSS-levelling dataset to determine the VDO from the NGF-IGN69 to the global height system (Vu et al. 2021b). This VDO value is required to determine the GIRAFE gravity anomalies in the national height system (as already discussed in Sect. 2.1). The local GNSS-levelling data are also employed to find the most suitable global gravity field model (GGM) and its optimal cut-off degree for the regional gravimetric quasigeoid calculation and the GIRAFE gravity downward continuation using the remove–compute–restore (RCR) technique on the study region. This procedure will be presented in the next section.

Finally, the GNSS-levelling data in the research region are employed to validate the estimated gravimetric quasigeoid models. The distribution of 39 co-located GNSS-levelling points in the Bay of Biscay is shown in Fig. 1a (red triangles). The quality of GIRAFE data has already been assessed based on two different metrics in Bidel et al. (2020, 2023): self-crossover calculation, i.e. difference at the intersection points, and comparison with surface gravity data after upward continuation. The details on technical performances and limitations of GIRAFE instrument were given in these papers. Here, our aim is to use the high-accuracy local GNSS-levelling data as external validation to quantify the contribution introduced by GIRAFE absolute airborne gravity data to the gravimetric quasigeoid model.

3 Quasigeoid computation methodology

The RCR procedure (Barzaghi 2016) is a well-known technique in regional geoid/quasigeoid modelling. In the present study, the RCR technique is employed to determine the gravimetric geoid/quasigeoid model from heterogeneous gravity data. This technique is also used to downward continue the GIRAFE data (see Sect. 4). In the first step, the residual gravity anomaly (Δg_{res}) is computed by removing the contribution of low and high frequencies from the surface gravity anomaly (Δg_{FA}). The goal of this step is to produce smooth gravity data for the gravimetric quasigeoid calculations. The remove step is performed as follows:

$$\Delta g_{res} = \Delta g_{FA} - \Delta g_{GGM} - \Delta g_{RTM} \tag{3}$$

where Δg_{GGM} is the low frequencies of gravity anomaly calculated employing a GGM, and Δg_{RTM} denotes the RTM (residual terrain model) effects (Forsberg 1984) on the gravity anomaly computed employing a DTM (digital terrain model).

After removing the low and high frequencies, the obtained residuals are much smoother than the original surface gravity anomalies. The GRAVSOFT/GEOGRID program is used to interpolate the smooth residual on a regular grid (see Sect. 4.2) (Forsberg and Tscherning 2008). This residual grid is then used to determine the residual height anomaly (ζ_{res}) employing Stokes' integration with the 1D-FFT spectral method (Haagmans et al. 1993) deployed by GRAVSOFT/SPFOUR program with the Wong–Gore (WG) modification of the Stokes' kernel (Wong and Gore 1969). The procedure for selecting the optimal degrees to modify the Stokes' kernel is presented in Sect. 5. Finally, the residual height anomalies (ζ_{res}) are restored the contribution of low and high frequencies by adding the height anomaly computed from a GGM and the terrain effects on the height anomaly to obtain the quasigeoid as follows:

$$\zeta = \zeta_{GGM} + \zeta_{RTM} + \zeta_{res} \tag{4}$$

where ζ_{GGM} denotes the height anomaly computed employing a GGM, ζ_{RTM} denotes the terrain effects on the height anomaly.

The GRAVSOFT/TC program was used to compute the terrain effects with the DTM using a radius of 20 km for the detailed grid and 200 km for the coarse grid. The DTM SRTM3arc_v4.1 with resolution of $3''$ (Farr et al. 2007) and the DBM (Digital Bathymetry Model) SRTM15arc_plus with resolution of $15''$ (Tozer et al. 2019) were used as the detailed grid over land and sea, respectively. After re-gridding to $3''$, the SRTM15arc_plus was merged with SRTM3arc_v4.1, called the mixed SRTM3/SRTM15 model, employing the full-resolution coastline in Generic Mapping Tools (GMT) (Wessel et al. 2019). A simple averaging is used to compute the coarse grid (e.g. $3' \times 3'$ grid in this study) from the high-resolution mixed SRTM3/SRTM15 model. A moving-average window is finally used to low-pass filter the coarse grid to the required resolution of reference DTM grid (Vu et al. 2019). The required resolution of the reference DTM grid is 9 km (equivalent to spherical harmonic degree/order (d/o) 2190 of the GGM; see below) for both gravimetric quasigeoid calculation and the downward continuation procedure in the present study.

All quasigeoid calculations were performed with the reference ellipsoid GRS80 and the mean tide system. The French national height system refers to the mean tide system (Liebsch et al. 2015); therefore, no conversion is required for local GNSS-levelling data.

The choice of a suitable GGM and its best maximum spherical harmonic degree to combine with RTM effects in the RCR procedure plays a vital role in determining the gravimetric geoid/quasigeoid. We used the local GNSS-levelling data to determine the best choice by comparing them with two recent releases of satellite-only GGMs (R5 and R6) enhanced with EGM2008 and RTM effects. The following GGMs were evaluated: DIR-R5 and DIR-R6 (Bruinsma et al. 2014), GOCO05s and GOCO06s (Mayer-Gürr et al. 2015; Kvas et al. 2021) and TIM-R5 and TIM-R6 (Brockmann et al. 2014, 2021). The differences in height anomaly for all these models from degree 100 up to the maximum degree n_{max} in steps of 10 degrees and the co-located GNSS-levelling points were evaluated following a spectral enhancement method as follows (Vergos et al. 2016):

$$\Delta \zeta = \zeta^{GNSS/levelling} - \zeta^{GGM\_S}\big|_2^{n_1}$$
$$- \zeta^{EGM2008}\big|_{n_1+1}^{2190} - \zeta^{RTM}\big|_{2191}^{216,000} - \zeta_0 \tag{5}$$

where $\Delta \zeta$ denotes the differences in height anomaly between the local GNSS-levelling data and the GGM plus terrain effects. $\zeta^{GGM\_S}\big|_2^{n_1}$ denotes satellite-only GGM-derived height anomalies. n_1 is the cut-off degree for which satellite-only GGMs are assessed. The goal of this evaluation is to determine the optimal cut-off degree of the satellite-only GGMs in combination with EGM2008. EGM2008-derived height anomalies from degree $n_1 + 1$ to degree 2190 ($\zeta^{EGM2008}\big|_{n_1+1}^{2190}$) along with RTM effects on height anomalies ($\zeta^{RTM}\big|_{2191}^{216,000}$) are used to fill-in information. Thanks to the RTM effects, the height anomaly spectrum is up to $3''$ (equivalent to d/o 216,000). ζ_0 denotes the zero-degree term. Figure 2 shows SD of the differences in height anomaly between the local GNSS-levelling data with the spectral enhancement approach of the satellite-only GGMs for various degrees of expansion. The latest R6 satellite-only model shows an improvement of 2 mm compared with the release 5

at degree 180. The reference model EGM2008 at degree $n_{\max}$ plus RTM effects provides a SD of 0.040 m, while that of the spectral enhancement approach with the satellite-only GGMs is 0.035 m for all three R6 models: DIR-R6, GOCO06s and TIM-R6. An improvement of 5 mm by GOCE compared with the EGM2008 model can be regarded as significant because most gravity data over France have been employed in its construction, i.e. the local data do not provide more accurate information than satellite gravity data at the long and medium wavelengths. Improvement due to GOCE data will be more important for regions where surface gravity data are unavailable. The smallest SD of all satellite-only GGMs is reached at degree 180.

The three R6 models have the same accuracy at degree 180 when compared with GNSS-levelling data in France. The DIR-R6 model, up to d/o 180, enhanced with EGM2008 up to d/o 2190, called the mixed DIR-R6/EGM2008 model, is selected as reference model in the RCR technique for both quasigeoid calculation and downward continuation procedure.

4 Airborne data processing and validation of available gravity data

4.1 Airborne gravimetry downward continuation

The altitude of the airborne GIRAFE measurements differs from that of the available surface gravity data. These gravity data have inhomogeneous spatial resolution and coverage. Therefore, prior to gravity field modelling, downward continuation (DC) of GIRAFE data from the aircraft's altitude to the topographic/sea surface is needed before they are merged with the surface gravity measurements in order to construct a gravity dataset with a more uniform spatial resolution. Numerically, DC methods can be classified as space- or frequency-domain procedures, including: least-squares

collocation (LSC) (Forsberg 1987), inverse Poisson's integral equation (Martinec 1996), direct band-limited approach (Novák et al. 2001) and the semi-parametric method (Zhao et al. 2017). We used the LSC method adapted to the RCR approach to DC airborne gravity data because it has several advantages (Barzaghi et al. 2009; Varga et al. 2021). This method does not require gridded input data or data at the same height. Similar to the RCR technique in quasigeoid computation, GGM and topographic information from the RTM effects were utilized to remove and restore low and high frequencies before and after the DC procedure, respectively. Initially, the gravity anomalies obtained from the mixed DIR-R6/EGM2008 model up to d/o 2190 were employed to remove and restore the low frequencies in the GIRAFE data. The terrain effects from RTM were estimated from the high-resolution mixed SRTM3/SRTM15 model to remove and restore the high frequencies in the GIRAFE data (beyond d/o 2190), i.e. those frequency components that remain after low-frequency reduction with a GGM. Then, the residual anomalies were downward continued to the topographic/sea surface employing the LSC method. This method requires an optimal covariance model that is in reasonable accordance with the spectral properties of the actual gravity field. As we know that the gravity field of Earth follows Kaula's rule, the covariance model must follow this rule too. We used the covariance model of Forsberg (1987), called attenuated planar logarithmic model, which was designed for downward or upward continuation of gravity anomalies. The GRAVSOFT/GPCOL1 program is used to downward continue the GIRAFE data from the aircraft's altitude to the topographic/sea surface. The DC estimation was performed according to the diagram in Fig. 3 in point-to-point mode.

In Fig. 3, $\Delta g_{\mathrm{FA}}^{\mathrm{air}}$ and $\Delta g_{\mathrm{res}}^{\mathrm{air}}$ denote free-air airborne gravity anomalies and their residuals, respectively. $\Delta g_{\mathrm{GGM}}^{\mathrm{air}}$ and $\Delta g_{\mathrm{GGM}}^{\mathrm{sur}}$ denote the low-frequency components in gravity anomaly data computed with the mixed DIR-R6/EGM2008 at the aircraft's altitude and at the topographic/sea surface, respectively. $\Delta g_{\mathrm{RTM}}^{\mathrm{air}}$ and $\Delta g_{\mathrm{RTM}}^{\mathrm{sur}}$ denote the terrain effects
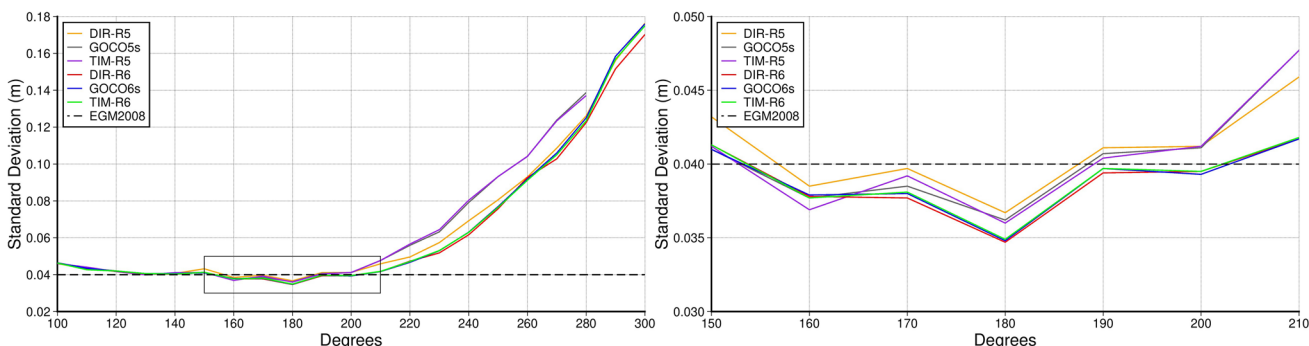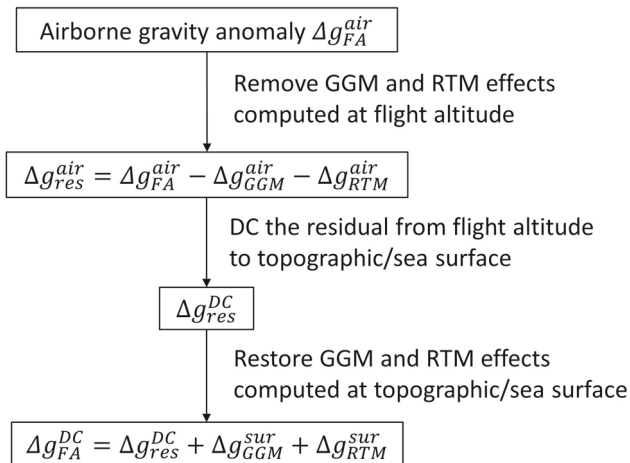

Fig. 2 Left) Standard deviation of the discrepancies in height anomaly between the local GNSS-levelling data with the spectral enhancement approach of the two releases satellite-only GGMs (R5 and R6) for various degrees of expansion, and Right) zoom in between degrees 150–210

Table 2 Statistics of RTM effects and airborne gravity anomaly before and after DC. Unit: (mGal)

Gravity anomaly	Mean	SD	Min	Max
RTM effects at flight altitude (Δg_{RTM}^{air})	− 0.13	1.06	− 6.55	3.78
RTM effects at topographic surface (Δg_{RTM}^{sur})	− 0.15	1.73	− 12.40	6.40
At flight altitude (before DC) (1)	− 0.81	25.48	− 90.50	39.97
At surface (after DC) (2)	− 0.92	28.29	− 101.15	47.72
(2)-(1) in absolute sense	1.87	2.65	− 6.62	11.93

Airborne gravity anomaly Δg_{FA}^{air}

Remove GGM and RTM effects computed at flight altitude

$\Delta g_{res}^{air} = \Delta g_{FA}^{air} - \Delta g_{GGM}^{air} - \Delta g_{RTM}^{air}$

DC the residual from flight altitude to topographic/sea surface

Δg_{res}^{DC}

Restore GGM and RTM effects computed at topographic/sea surface

$\Delta g_{FA}^{DC} = \Delta g_{res}^{DC} + \Delta g_{GGM}^{sur} + \Delta g_{RTM}^{sur}$

Fig. 3 Diagram of steps in the DC of GIRAFE data to the Earth's surface

at the aircraft's altitude and at the topographic/sea surface, respectively. The low and high frequencies are determined at both altitudes in remove/restore steps in the DC procedure. Δg_{FA}^{DC} and Δg_{res}^{DC} denote DC gravity anomalies and their residual values, respectively. Table 2 lists the topographic effects at both altitudes. The influence of topography is not so strong since the area is relatively flat. In general, the topographic effects decrease with height. Their range (maximum–minimum value) is 10.33 mGal at the flight altitude (1500 m) compared with 18.80 mGal on the topographic/sea level. The RTM effects play an important role in DC procedure (see Forsberg et al. 2007; Hsiao and Hwang 2010; Zhao et al. 2018; Vu et al. 2024). The application of RTM effects significantly improved the accuracy of the DC airborne gravity anomalies especially over mountainous areas. Zhao et al. (2018) indicated that about ¾ of DC errors are due to the quality of RTM effects. On the other hand, we can hardly see significant improvements when using RTM effects in the relatively flat regions such as coastal zones (Wu et al. 2019). Here, we do not focus on the assessment of RTM effects in DC procedure. However, to accommodate the use of RCR technique in the quasigeoid determination, we used the RTM effects in the DC procedure.

After removing GIRAFE airborne data during periods of significant variation in roll, pitch and heading angles, the free-air gravity anomalies before/after DC are listed in Table 2 and

shown in Fig. 4. The land, shipborne and airborne datasets were assigned a priori errors of 1, 2 and 2 mGal, respectively. Table 2 indicates that the DC gravity anomalies on the surface have a mean value of − 0.92 mGal, a SD value of 28.29 mGal, a minimum of − 101.15 mGal and a maximum of 47.72 mGal, whereas corresponding values at the flight altitude are − 0.81, 25.48, − 90.50 and 39.97 mGal. Compared with gravity anomalies at the flight altitude, the signatures of the DC gravity anomalies are more prominent due to the influence of topography at the surface (see Table 2). After DC to the Earth's surface, the magnitudes of airborne gravity anomalies become larger as the measuring point is closer to the mass. A disadvantage of DC is that it amplifies the short-wavelength noise in the airborne data (Li et al. 2022). However, this noise amplification of high frequencies will be offset by the gravity to geoid/quasigeoid low-pass filtering operation.

The residual GIRAFE DC anomalies were merged with the residual surface gravity data for gravimetric quasigeoid calculations.

4.2 Comparison with available gravity data

The GIRAFE DC gravity anomalies are used to assess the available gravity data in the study region, including gravity data derived from DTU, UCSD series models and surface data. These available gravity data are interpolated to the positions of the airborne observations using the LSC approach in GRAVSOFT/GEOGRID program for comparison with the GIRAFE DC gravity anomalies. Table 3 shows the main results of the comparison, showing SD ranging from 2.55 to 4.61 mGal. As expected, DTU series models compare better than UCSD because they are more accurate in coastal areas (see Fig. 5a and b). The SD of UCSDv31 is 1.56 mGal larger than that of DTU21 when compared with GIRAFE. Figure 5c shows the spatial behaviour of a subset of the comparison made with the DC GIRAFE gravity anomalies. This figure reveals a large bias over sea (− 4.00 mGal) compared with over land (− 0.73 mGal), which is most likely due to the tie point reference value on land and drift in relative gravimeters used to collect gravity observations during terrestrial and shipborne surveys. Such a bias is not present in Fig. 5a and b for altimetric gravity data. We decided to eliminate
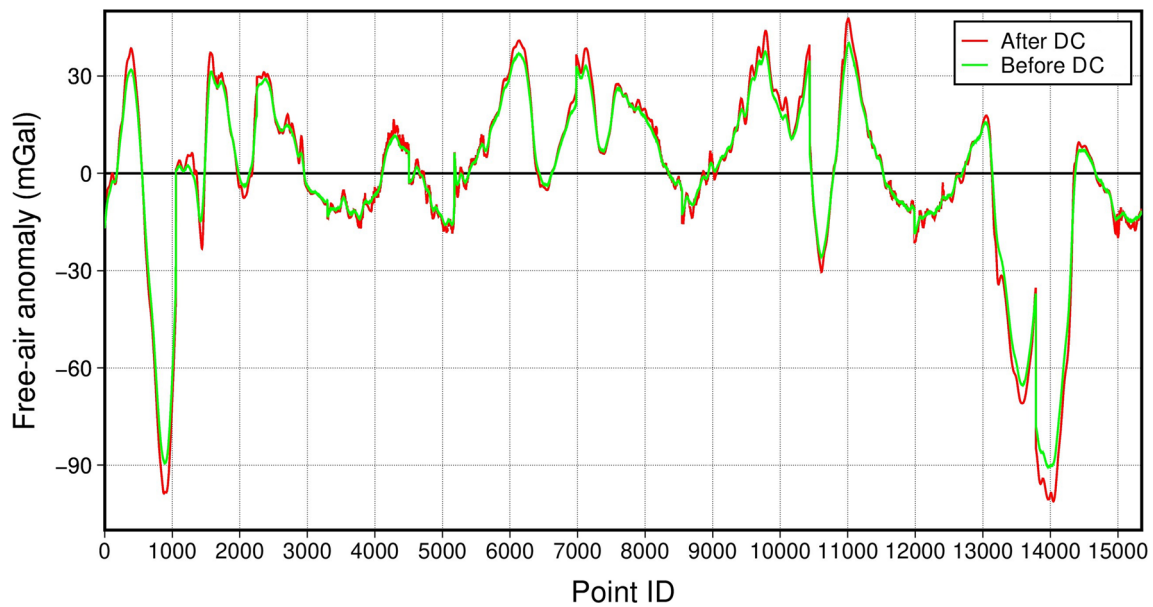
Fig. 4 Free-air airborne gravity anomalies before and after DC. Point IDs represent the point numbers

Table 3 Statistics of the discrepancies in gravity anomaly between the DC GIRAFE and interpolated altimetric DTU and UCSD series models, and available surface gravity data. Unit: (mGal)

Data	Mean	SD	Min	Max
DC GIRAFE-DTU21	− 0.57	2.55	− 10.00	12.37
DC GIRAFE-DTU17	− 0.77	3.11	− 14.73	11.93
DC GIRAFE-DTU15	− 0.82	2.95	− 12.65	11.00
DC GIRAFE-UCSDv31	− 1.04	4.11	− 22.35	12.92
DC GIRAFE-UCSDv29	− 1.26	4.57	− 33.13	16.84
DC GIRAFE-UCSDv27	− 1.15	4.31	− 23.56	13.73
DC GIRAFE-UCSDv25	− 1.31	4.61	− 25.79	13.95
DC GIRAFE-Surface	− 3.00	3.24	− 12.97	10.94
DC GIRAFE-Surface (debiased)	0.00	2.88	− 10.15	14.88

the biases in the shipborne and terrestrial gravity data (DC GIRAFE-Surface (debiased), Fig. 5d), which reduces the SD of the differences from 3.24 to 2.88 mGal (Table 3). Using the differences at the intersection points between traverse and tie lines, the accuracy of GIRAFE is determined to be around 1–1.5 mGal (Bidel et al. 2023). With an observed SD of around 3 mGal between altimetric models and GIRAFE observations over sea, this means that the accuracy of the altimetric models must be around 2.5–2.8 mGal in the study area. This accuracy of the altimetric models is consistent with Rouxel et al. (2023), in which they were compared with shipborne gravity data on the Atlantic Ocean.

Examination of the statistics of each model series reveals the improvement of the altimetric models as a function of the amount of altimetry data used in their realization. However, the DTU17 and UCSDv27 models do not improve compared with the previous release, i.e. DTU15 and UCSDv25, respectively, they are even worse over some part of the study area.

Andersen and Knudsen (2020) indicated that the improvement of DTU17 compared with DTU15 can only be seen in the coastal zone. In the depth variation of 500–2000 m, DTU17 is worse than DTU15. Hence, to further investigate the improvement of the altimetric models with depth, we have split the evaluation between the GIRAFE data and various available gravimetry into sub-comparisons along the west–east tracks of airborne measurements.

As with surface gravity data, we also apply debiasing to the DTU and UCSD series models to avoid undesirable effects in model comparison. The difference between the DC GIRAFE gravity anomalies and those interpolated from altimetric DTU and UCSD series models, and available surface gravimetry are shown in Fig. 6, with (right frames) and without debiasing (left frames). Line numbers are shown in Fig. 5a. Figure 6 highlights the contribution of recent satellite altimeter missions in the improvement of the altimetric models in coastal zones. The newer models are more accurate than
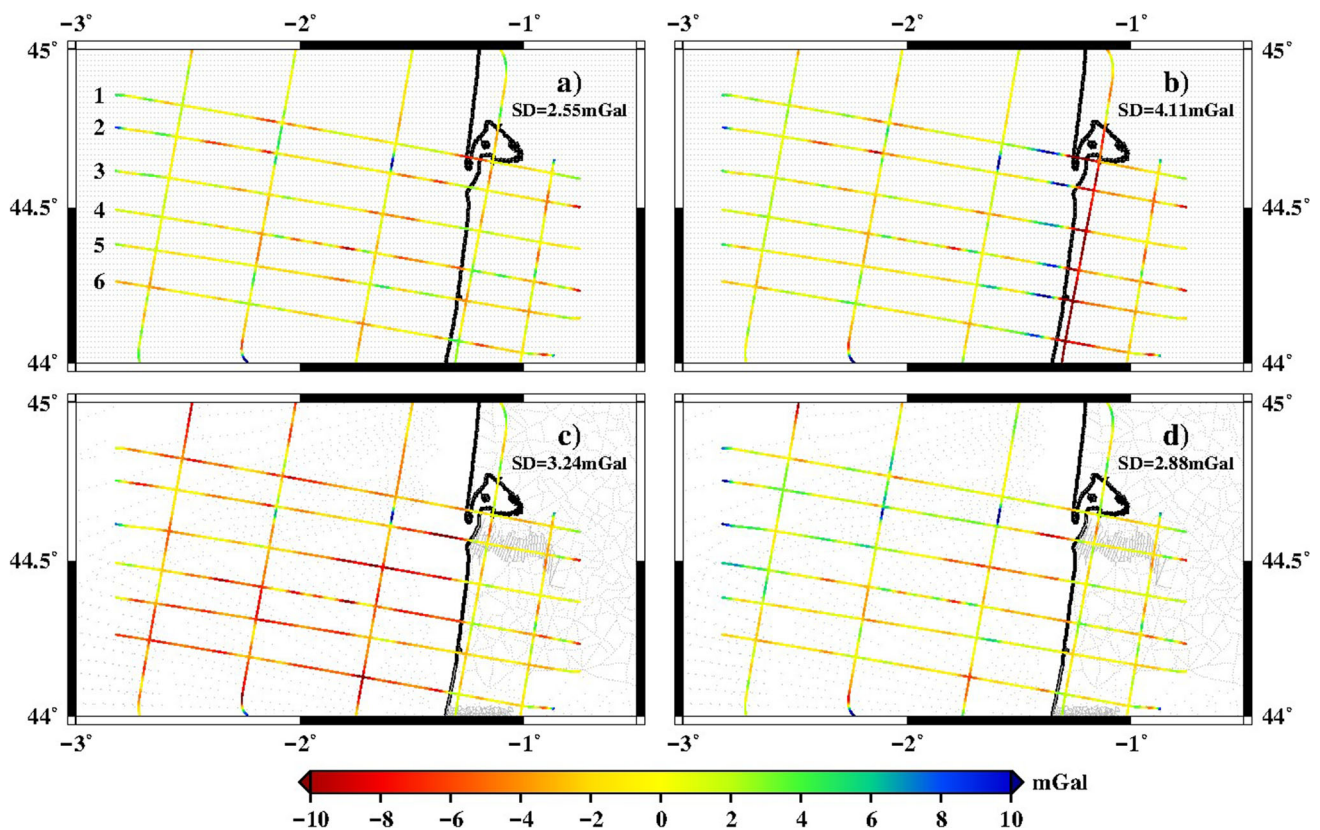
Fig. 5 Differences between the DC GIRAFE and gravity anomalies interpolated from: **a** altimetric model DTU21; **b** UCSDv31 and **c** available surface gravity data. Figure **d** likes (c) but gravity data were debiased. Line numbers are shown in (a)

their predecessors. The gravity anomalies derived from two series models differ significantly near the coast. The accuracy of DTU models in the coastal zones is comparable to that further offshore as well as comparable to the shipborne data, while the UCSD models are significantly worse. It should also be noted that the availability of land gravity data along the coastal areas in the reference fields (i.e. EGM2008) has substantially improved the accuracy of the altimetric gravity field models, particularly in the DTU models. This is the case for this study area, for which land gravity data were available and ingested in EGM2008. Except for the Arcachon Bay (line 1, see Fig. 5a), a small inland sea, the difference of DTU models with GIRAFE data in coastal zones is about 5 mGal while with UCSD models it is more than 10 mGal. In contrast, the UCSD models tend to be more accurate when going further away from the coast, especially in the large depth region in the northwestern part of the study region (lines 1, 2 and 3). However, the accuracy of the altimetric models is significantly reduced on land when compared with the results from the terrestrial data (black lines) even though this terrestrial database is consistent with that used in these altimetric models, i.e. EGM2008 as mentioned. This proves that the poor quality of near-coastal altimetric data has significantly contaminated the grid data over land in the altimetric models

when using these altimetric models to interpolate to GIRAFE measurement points. Concerning ship gravity data, the discrepancies in gravity anomaly compared with DC GIRAFE are large in areas where the shipborne data are less dense, such as the coastal zone of lines 2 and 3, and the northwestern part of lines 2, 3 and 4; this difference is not so large for these areas with the altimetric models. The northwestern part is much deeper than the rest of the study area, which seems to indicate that the large differences over these areas are due to noisy shipborne data. Moreover, the discrepancy in gravity anomaly between the DC GIRAFE and interpolated surface gravity data (black lines) shows that more significant signals are found over sea than over land. Considering the homogeneous quality of GIRAFE data, it is due to the lower quality and distribution of shipborne gravity data compared with land data. All these comparative results demonstrate the possibility of GIRAFE to quantify and validate available gravity data in land–sea transition areas.

The gravity anomaly models were created as follows:

- The mixed DIR-R6/EGM2008 model from degrees 2–2190 and terrain effects from degrees 2191–216,000 at the topographic surface is employed to remove low and
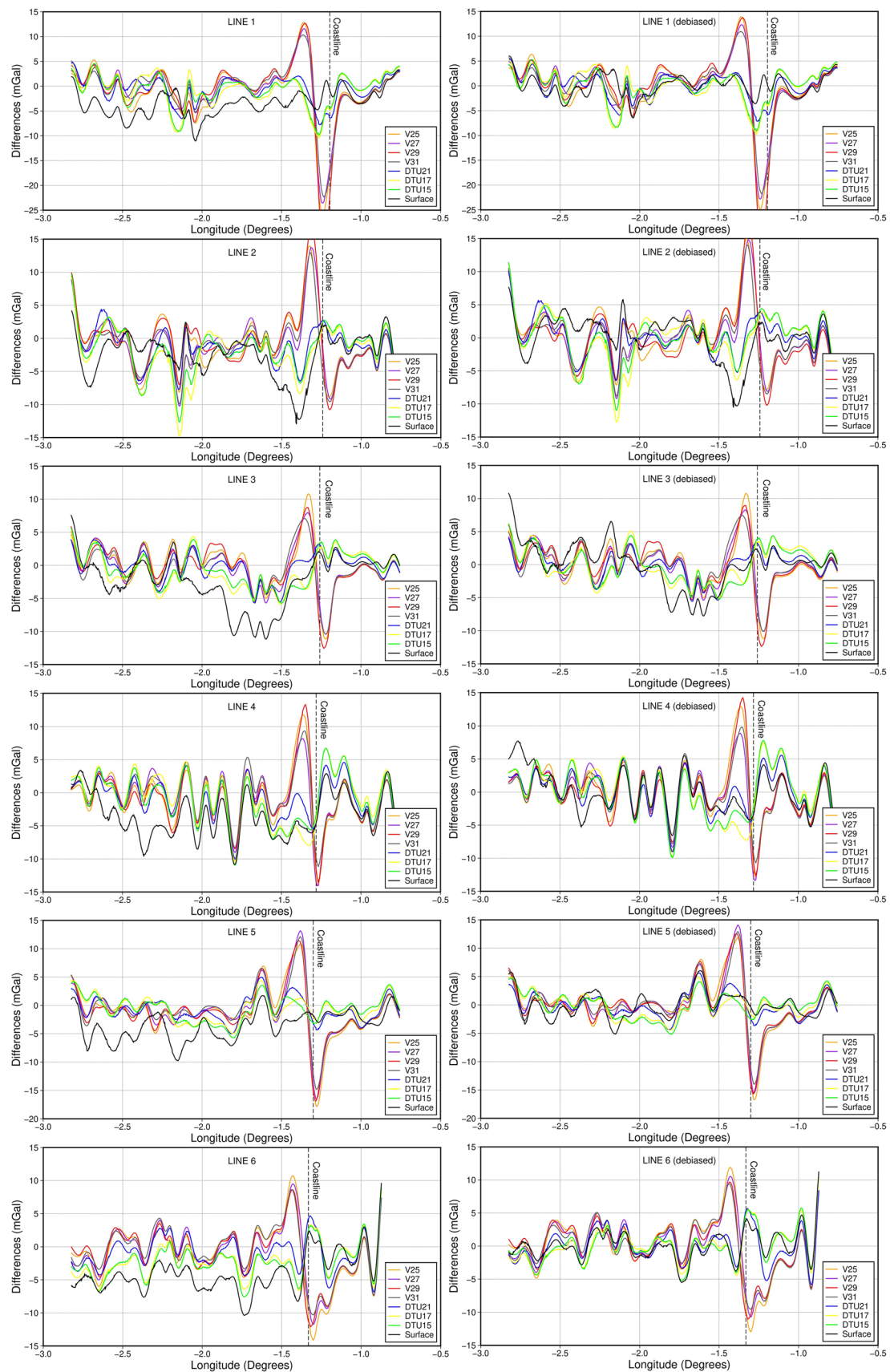
Fig. 6 Differences, on each west–east measuring line, between the DC GIRAFE gravity anomalies and those interpolated from altimetric DTU and UCSD series models, and available surface gravity data. Left frames) Before debiasing, and Right frames) After debiasing. From top to bottom corresponds to the measuring lines numbered from 1 to 6 (see Fig. 5a)
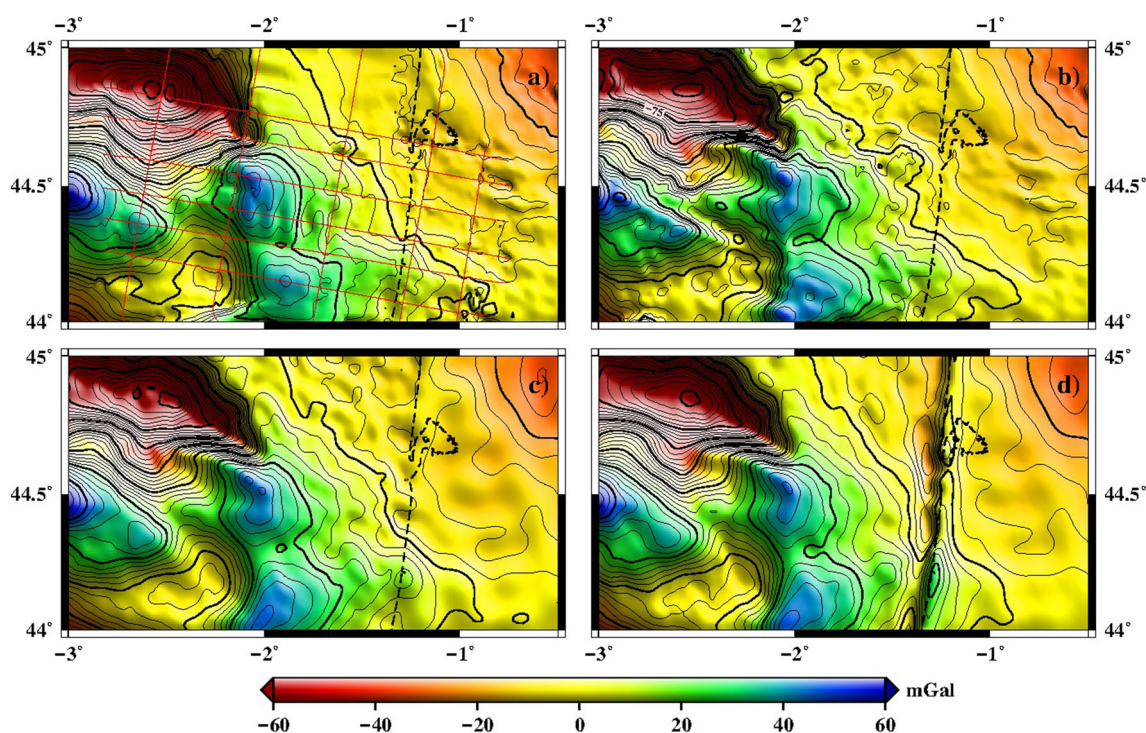
Fig. 7 Gravity anomaly model on the Bay of Biscay (grid of 1'): **a** Model obtained with GIRAFE plus terrestrial gravity; **b** Model obtained with debiased surface gravity; **c** Model obtained with DTU21; and d) Model obtained with UCSDv31

high frequencies in the ground-based gravity data, respectively.

- The residual ground data are then merged with the residual DC GIRAFE data to interpolate onto a regular grid of 1' using the LSC method with the GRAVSOFT/GEOGRID program and a priori errors of 1 and 2 mGal for the land and airborne gravity datasets, respectively. A correlation length of the covariance function of 10 km was used. This residual merged grid was used to estimate the quasigeoid model.

- To model the gravity fields for the study area, this residual grid is restored by adding the mixed DIR-R6/EGM2008 model and terrain effects at the topographic surface calculated at the location of grid nodes (see Fig. 7a). Similarly, the residual shipborne data are combined with the residual land data to model the gravity fields (Fig. 7b). The gravity field models obtained from the DTU21 and UCSDv31 are also shown in Fig. 7c and d, respectively.

The four models are similar but the shipborne and airborne models have a higher resolution. Inspection of Fig. 7a and b shows that GIRAFE data substantially improve the spatial resolution of the gravity models in the coastal area, and even onshore despite this being a flat area with relatively dense gravity data. However, in the upper left corner it seems that the resolution of GIRAFE data (Fig. 7a) is lower than that of the shipborne data (Fig. 7b) and even the altimetric gravity

data (Fig. 7c and d). This is probably due to the small number of GIRAFE airborne gravity lines in that region (see Fig. 1b) while the gravity anomalies are relatively rough there.

5 Regional quasigeoid modelling and validation

5.1 Regional quasigeoid modelling

From the residual merged grid computed in Sect. 4, the gravimetric quasigeoid models are determined on a regular grid with resolution $1' \times 1'$ from $44° \leq \varphi \leq 45°$ to $-3° \leq \lambda \leq -0.5°$. However, all gravimetric quasigeoid calculations in this study are carried out for an extended region $43° \leq \varphi \leq 46°$ and $-4° \leq \lambda \leq 0.5°$ to avoid edge effects. The UCSDv31 model and terrestrial gravity data are used on sea and land, respectively, in the extension. We computed eight regional quasigeoid solutions to quantify the contribution of GIRAFE. Table 4 describes the gravity data used to estimate these eight quasigeoid solutions. The land gravity data are used in all eight quasigeoid solutions.

In the RCR procedure for regional gravimetric quasigeoid determination, Stokes' integration is computed on a spherical cap using local gravity data with limited radius of 2° around the calculation point. For the outer zones, the mixed DIR-R6/EGM2008 GGM was used. Using a GGM causes

Table 4 Description of the regional gravimetric quasigeoid solutions

N°	Gravity data	Gravimetric quasigeoid name
1	Residual DC GIRAFE	QBC_GIRAFE
2	Residual DTU21	QBC_DTU21
3	Residual UCSDv31	QBC_UCSDv31
4	Residual shipborne gravity without debiased	QBC_shipborne
5	Residual debiased shipborne gravity	QBC_shipborne(db)
6	Residual DC GIRAFE merged DTU21 removing the grid points within 10 km from coastline	QBC_GIRAFE_DTU21(r)
7	Residual DC GIRAFE merged UCSDv31 removing the grid points within 10 km from coastline	QBC_GIRAFE_UCSDv31(r)
8	Residual DC GIRAFE merged debiased shipborne gravity	QBC_GIRAFE_shipborne(db)

truncation errors even when the most suitable model with an optimal cut-off degree has been carefully selected. The kernel of the Stokes integral must be modified by removing the low frequencies up to degree (N_1) and then linearly tapered to degree (N_2), to reduce these truncation errors (Forsberg and Tscherning 2008). Optimal degrees N_1 and N_2 vary from region to region, depending on the quality of the reference GGM and the local gravity data used. But these degrees should not exceed the n_{max} of the reference GGM. We conducted tests, similar to Vu et al. (2019), to find the optimum degrees for this study region. The gravimetric quasigeoid model was computed with GRAVSOFT/SPFOUR program employing WG modification with degrees (N_1 and N_2) tested from 50 to 180 (this is the maximum degree of the DIR-R6 used in the combination with EGM2008) in 10-degree steps. The local GNSS-levelling points are then used to assess the quasigeoid solutions. Finally, the best gravimetric quasigeoid solution is found when $N_1 = 100$ and $N_2 = 110$, and these values were used to calculate the gravimetric quasigeoid models.

After restoring the GGM and RTM effects, we obtained a gravimetric quasigeoid of the study area (see QBC_GIRAFE in Fig. 8a). The quasigeoid model is seamless in the sea–land transition area. The differences between QBC_GIRAFE_shipborne(db) with QBC_shipborne(db), QBC_GIRAFE_DTU21(r) with QBC_DTU21 and QBC_GIRAFE_UCSDv31(r) with QBC_UCSDv31 show the contribution of GIRAFE measurement in terms of anomaly heights, see Fig. 8b, c and d. This contribution reaches a level of 3 cm in terms of height anomaly for DTU21 while much larger for UCSDv31 and shipborne data, displaying more significant signals over sea than land. The largest differences are concentrated in the coastal areas. The reason may be the degraded quality of altimeter data processing and the lack of the shipborne data in coastal zones while the GIRAFE data are seamless. Onshore, the difference is less than 1 cm except for the UCSDv31 model. The use of GIRAFE data has significantly reduced

the contamination by UCSDv31 of the ground data. The land data provide good coverage and are of high quality over the Biscay Basin, and the improvement thanks to the GIRAFE data becomes less. Over sea, the differences are clearly visible along the flight tracks indicating the contribution of the GIRAFE data. For the shipborne data, the difference in height anomaly is consistent with the difference between the DC GIRAFE and shipborne data in Fig. 5d. The large differences between the QBC_GIRAFE_shipborne(db) and QBC_shipborne(db) are found for areas where the shipborne data are sparse, such as the open area of the Arcachon Bay (red signals in Fig. 8b), as well as the deep-water region in the northwest part of the study region (blue signals in Fig. 8b). However, the differences over these two zones are quite small when the altimetric models are used. This again is due to the lower quality of the ship gravity data, and consequently GIRAFE data lead to major improvements. For the altimetric models, a large difference is visible in the Arcachon Bay (red signals in Fig. 8c and d). This is a challenging region for satellite altimetry as it is a small inland sea characterized by shallow water.

5.2 Validation of the regional quasigeoids

High-quality co-located GNSS-levelling data are employed to validate the eight quasigeoid solutions in the Bay of Biscay. Table 5 and Fig. 9 show the validation results of eight quasigeoid models with GNSS-levelling data. The EGM2008 and QGF16 models are also used to compare with GNSS-levelling data to indicate the improvement of new models thanks to the GIRAFE data. The QGF16 was calculated in 2016 with a grid of 2′ in longitude and 1.5′ in latitude using the GRS80 ellipsoid. A set of 875,661 terrestrial and shipborne gravity points was used.

The statistical metrics indicate that the mean bias value of discrepancies in height anomaly between the GNSS-levelling data and the gravimetric quasigeoid models is around 6–7 cm, except for the QBC_UCSDv31 model, which is affected by
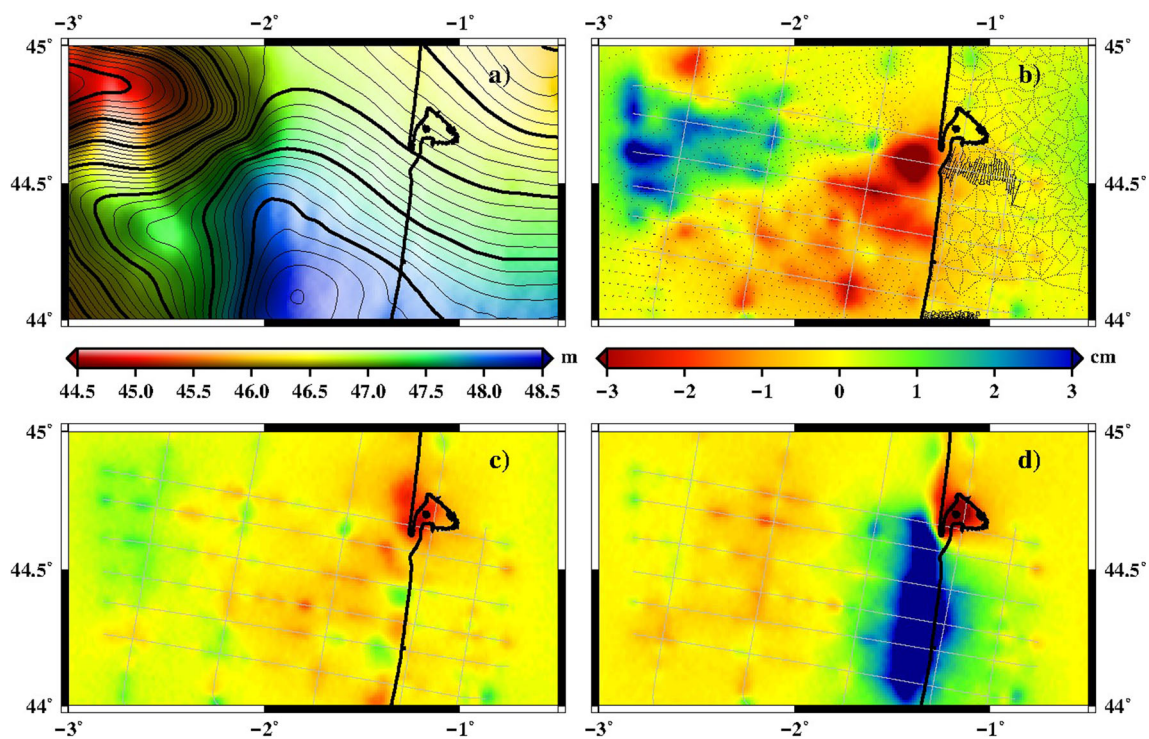
Fig. 8 **a** Gravimetric quasigeoid of the Bay of Biscay (grid of 1') calculated from GIRAFE plus terrestrial gravity QBC_GIRAFE; Contribution of GIRAFE data to the regional quasigeoid, i.e. differences between the solution calculated from the merged data with and without the GIRAFE data plus: **b** shipborne and terrestrial data: QBC_GIRAFE_shipborne(db) minus QBC_shipborne(db); **c** DTU21 and terrestrial data: QBC_GIRAFE_DTU21(r) minus QBC_DTU21; d) UCSDv31 and terrestrial data: QBC_GIRAFE_UCSDv31(r) minus QBC_ UCSDv31

Table 5 Differences between the GNSSlevelling points with the gravimetric quasigeoids calculated using different strategies for combining heterogeneous gravity data. Bold numbers represent good and bad standard deviations. Unit: (cm)

Data	All points (39 points)				Points near coast (14 points)			
	Mean	SD	Min	Max	Mean	SD	Min	Max
QBC_GIRAFE	− 6.4	**1.2**	− 9.1	− 4.2	− 6.9	**0.8**	− 8.4	− 5.2
QBC_DTU21	− 5.9	1.5	− 9.8	− 2.9	− 7.0	1.5	− 9.8	− 4.1
QBC_UCSDv31	− 10.0	2.2	− 14.6	− 4.7	− 11.0	1.9	− 14.6	− 8.0
QBC_shipborne	− 7.5	2.3	− 14.5	− 4.1	− 8.6	2.4	− 14.5	− 5.2
QBC_shipborne(db)	− 7.3	1.5	− 11.8	− 5.0	− 7.7	1.6	− 11.8	− 5.5
QBC_GIRAFE_DTU21(r)	− 6.7	**1.2**	− 9.5	− 4.3	− 7.1	**0.8**	− 8.6	− 5.9
QBC_GIRAFE_UCSDv31(r)	− 6.1	**1.1**	− 8.8	− 4.2	− 6.2	**0.8**	− 7.7	− 5.1
QBC_GIRAFE_shipborne(db)	− 5.8	**1.0**	− 8.3	− 3.7	− 6.7	**0.8**	− 8.2	− 5.8
QGF16	− 21.6	**3.8**	− 28.8	− 11.2	− 23.3	**2.2**	− 28.8	− 20.4
EGM2008	− 7.6	**2.4**	− 13.6	− 2.4	− 9.2	**2.4**	− 13.6	− 5.7
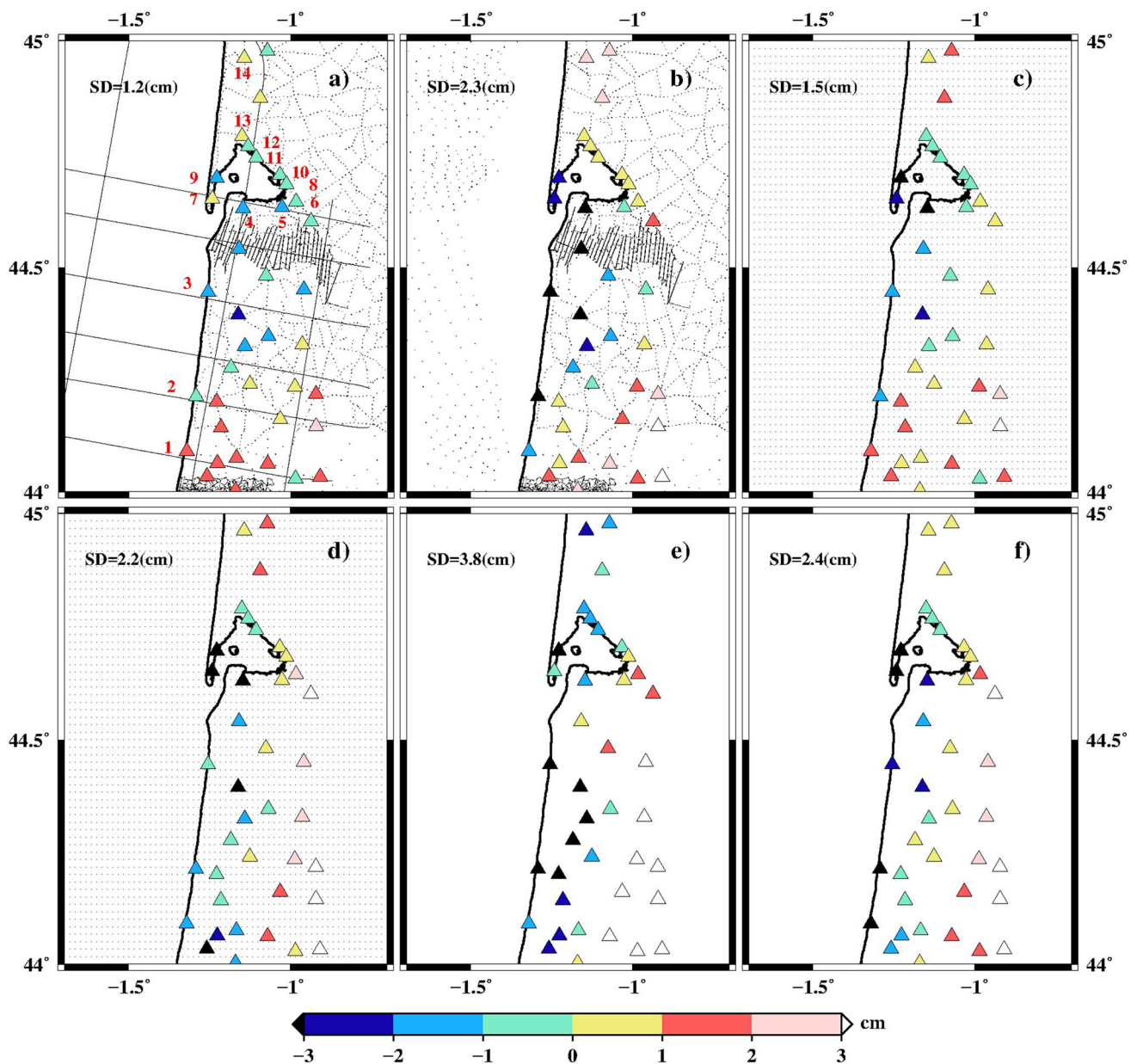
Fig. 9 Discrepancies in height anomaly between the GNSS-levelling data and the gravimetric quasigeoid: **a** QBC_GIRAFE; **b** QBC_shipborne; **c** QBC_DTU21; **d** QBC_UCSDv31; **e** QGF16 and **f** EGM2008. The mean value was removed from these differences

the poor quality of UCSDv31 in the coastal zone (see blue signals near the coast in Fig. 8d). These mean bias values are comparable with the one obtained with EGM2008 (− 7.6 cm). Large differences in mean bias between QBC models and QGF16, about − 7 cm against − 21.6 cm, may be due to the different tide system used and/or the zero-degree term. This information is not disclosed in QGF16 (L'Écu 2017). Here the zero-degree term is not included in the mean biases of QBC models and EGM2008. Hence, the mean bias values between the all quasigeoid models (Biscay, France and

EGM2008) and GNSS-levelling data are removed to avoid undesirable effects for model comparison.

The results of the validation with GNSS-levelling points in Table 5 and Fig. 9 indicate the contribution of GIRAFE data. The highest accuracy is achieved when GIRAFE data are merged with refined gravity data, i.e. debiased shipborne data, or by removing the grid nodes near the coastline in altimetric models. Slightly better results are obtained when the debiased shipborne data are merged with the GIRAFE data: SD of 1.0, 1.1 and 1.2 cm for QBC_GIRAFE_shipborne(db),
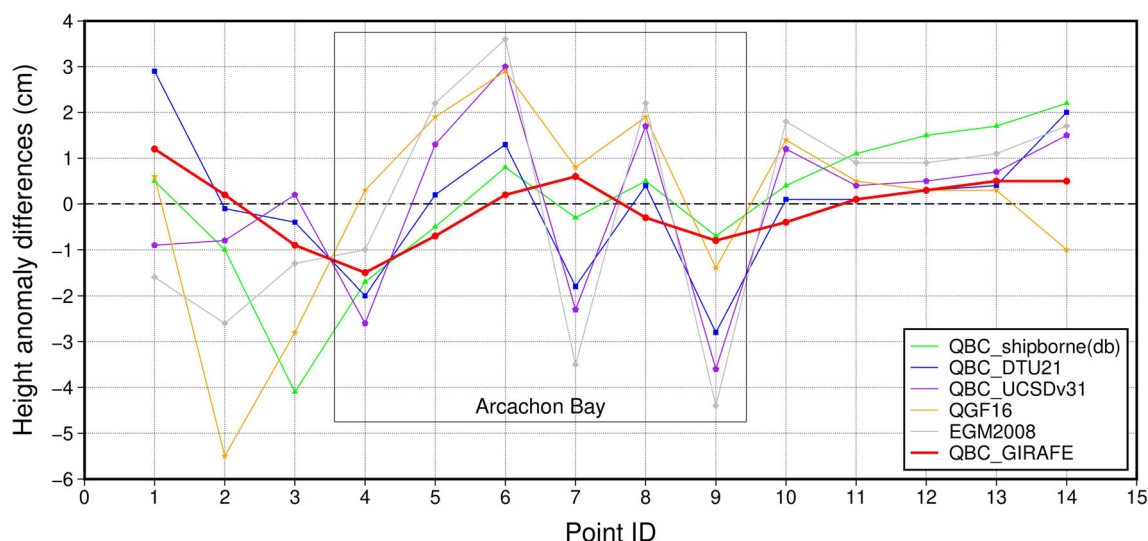
Fig. 10 Differences on 14 points near the coast between the GNSS-levelling points with the quasigeoid computed using different data or models. Point IDs numbered in Fig. 9a. The mean value was removed from these differences

QBC_GIRAFE_UCSDv31(r) and QBC_GIRAFE_DTU21(r), respectively. These models are much more accurate than QGF16 and EGM2008: SD of 3.8 and 2.4 cm, respectively. The new French quasigeoid model (QGF16) is worse than EGM2008 in the study region. We suspect that it is due to biases in the shipborne data that have not been handled well in QGF16. The improvement of QBC_DTU21 compared with EGM2008, SD of 1.5 against 2.4 cm, is due to the use of the new DTU21 model (EGM2008 used DNSC07 for coastal zones (Pavlis et al. 2012)). This once again proves the contribution of recent satellite altimetry missions to obtaining more accurate quasigeoid models. Importantly, even if only GIRAFE data are used over sea, the SD is 1.2 cm, which is equivalent to the combined models when compared with local GNSS-levelling points. Note that 1 cm accuracy is currently the goal in determining geoid/quasigeoid model in modern geodesy (Wang et al. 2021). Our results also show the correctness of the bias reduction of the ship gravity data. The accuracy of the quasigeoid increases by 0.8 cm (34.8%), 1.5 cm against 2.3 cm, when the debias procedure is applied. This confirms that the shipborne observations must be treated with care before using them. However, the accuracy of QBC_shipborne(db) is still worse than QBC_GIRAFE, mainly due to the discrepancies observed in the points located in the coastal strip, which is likely due to the lack of ship data there. A south–north tilt in height anomaly differences between the GNSS-levelling data with QBC_GIRAFE model is visible in Fig. 9a, but is not obvious in the other frames. The French height system (NGF-IGN69) is known for its tilt in the south–north direction (Denker 1998), and it explains the trend seen in Fig. 9a.

5.3 Validation of regional quasigeoids along the coastal strip

From the 39 GNSS-levelling points, we selected 14 in the coastal strip (the red numbers in Fig. 9a) to evaluate the contribution of GIRAFE data to the resulting quasigeoid models. The main results of this evaluation are shown in Table 5 and in Fig. 10. The quasigeoid models (QBC_GIRAFE, QBC_GIRAFE_DTU21(r), QBC_GIRAFE_UCSDv31(r), QBC_GIRAFE_shipborne(db)) using GIRAFE data have an accuracy of 0.8 cm. The QBC_GIRAFE_DTU21(r), QBC_GIRAFE_UCSDv31(r) and QBC_GIRAFE_shipborne(db) provide an improvement of 46.7%, 57.9% and 50% compared with QBC_DTU21, QBC_UCSDv31 and QBC_shipborne(db), respectively. The SD of the selected 14 GNSS-levelling points is smaller than that of all 39 GNSS-levelling points for these models. In contrast, the SD of the 14 points is larger than or equal to that of all 39 points for the quasigeoid models without using GIRAFE data. This means that the accuracy of quasigeoid models using GIRAFE data is not degraded in the near-coast land regions. The precision of QGF16 is equivalent to the quasigeoids calculated using the shipborne data without debiased plus land gravity data (i.e. QBC_shipborne), SD of 2.2 and 2.4 cm for QGF16 and QBC_shipborne, respectively. This again proves that the shipborne data used in QGF16 have not been debiased. Figure 10 clearly shows that even using the GIRAFE data only over sea leads to quasigeoid accuracy that is higher than that of the other models calculated using DTU21, UCSDv31 and shipborne data or QGF16 and EGM2008 models. In particular, the points in the Arcachon Bay (black square in Fig. 10), two models calculated with altimetric gravity data (QBC_DTU21 and

QBC_UCSDv31) have poor accuracy, which again indicates the lower quality of the altimetric gravity models there.

6 Conclusions and perspectives

Our results clearly show the great potential of GIRAFE data for improving the accuracy in the determination of the coastal gravity field and for quasigeoid modelling. Comparison with the GIRAFE data allows us to recommend the use of DTU models rather than UCSD models when working in coastal regions in the Bay of Biscay. The large bias (-4.00 mGal) found in shipborne gravity data makes it difficult to use these data, and a pre-processing stage is required. The correctness of debiased shipborne data was validated in this study. This suggests that independent gravity data should be used to detect biases in shipborne data. Airborne absolute gravity data is optimal for this purpose.

To investigate the contribution of GIRAFE data in determining gravimetric quasigeoids, eight models were calculated for the Bay of Biscay. The local GNSS-levelling points were used to compare with the quasigeoid models. The GIRAFE data improved the accuracy of the gravimetric quasigeoid solutions by approximately 50%. The highest accuracy, around 1 cm, is achieved when GIRAFE data are merged with refined available gravity data, i.e. debiased or by removing points near the coastline in altimetric models. Importantly, even if only GIRAFE data are used over the ocean, the SD increases only slightly to 1.2 cm when compared with GNSS-levelling data. Gravity field and gravimetric quasigeoid models constructed in this study are available via the BGI website.

Shipborne gravity data are scarce in coastal zones and gravity data are relatively sparse in the mountainous regions of France. Based on the compelling results of this study, future efforts to enhance the French quasigeoid models should take advantage of the new absolute gravimeter, GIRAFE, to improve the gravity field over land–sea transitions and inaccessible regions. Furthermore, airborne measurements over the coastal areas and up to 10 km from the coastline over sea are highly recommended to complement satellite altimetry. However, first a similar study on the potential of GIRAFE data to improve gravity fields over mountainous areas should be undertaken.

References

Abulaitijiang A, Andersen OB, Stenseng L (2015) Coastal sea level from inland CryoSat-2 interferometric SAR altimetry. Geophys Res Lett 42(6):1841–1847. https://doi.org/10.1002/2015GL063131

Andersen OB (1999) Shallow water tides in the northwest European shelf region from TOPEX/POSEIDON altimetry. J Geophys Res Oceans 104(C4):7729–7741. https://doi.org/10.1029/1998JC900112

Andersen OB, Knudsen P (1998) Global marine gravity field from the ERS-1 and Geosat geodetic mission altimetry. J Geophys Res Oceans 103(C4):8129–8137. https://doi.org/10.1029/97JC02198

Andersen OB, Knudsen P (2000) The role of satellite altimetry in gravity field modelling in coastal areas. Phys Chem Earth Part Solid Earth Geod 25(1):17–24. https://doi.org/10.1016/S1464-1895(00)00004-1

Andersen OB, Knudsen P (2020) The DTU17 global marine gravity field: first validation results. In: Mertikas SP, Pail R (eds) Fiducial reference measurements for altimetry. Springer International Publishing, Cham, pp 83–87

Andersen OB, Scharroo R (2011) Range and geophysical corrections in coastal regions: and implications for mean sea surface determination. In: Vignudelli S, Kostianoy AG, Cipollini P, Benveniste J (eds) Coastal Altimetry. Springer, Berlin, Heidelberg, pp 103–145

Barzaghi R (2016) The remove-restore method. In: Grafarend E (ed) Encyclopedia of geodesy. Springer International Publishing, Cham, pp 1–4

Barzaghi R, Borghi A, Keller K, Forsberg R, Giori I, Loretti I, Olesen AV, Stenseng L (2009) Airborne gravity tests in the Italian area to improve the geoid model of Italy. Geophy prospect 57(4):625–32

Bastos L, Cunha S, Forsberg R, Olesen A, Gidskehaug A, Timmen L, Meyer U (2000) On the use of airborne gravimetry in gravity field modelling: experiences from the AGMASCO project. Phys Chem Earth Part Solid Earth Geod 25(1):1–7. https://doi.org/10.1016/S1464-1895(00)00002-8

Bidel Y, Zahzam N, Blanchard C, Bonnin A, Cadoret M, Bresson A, Rouxel D, Lequentrec-Lalancette MF (2018) Absolute marine gravimetry with matter-wave interferometry. Nat Commun 9(1):627. https://doi.org/10.1038/s41467-018-03040-2

Bidel Y, Zahzam N, Bresson A, Blanchard C, Cadoret M, Olesen AV, Forsberg R (2020) Absolute airborne gravimetry with a cold atom sensor. J Geod 94(2):20. https://doi.org/10.1007/s00190-020-01350-2

Bidel Y, Zahzam N, Bresson A, Blanchard C, Bonnin A, Bernard J, Cadoret M, Jensen TE, Forsberg R, Salaun C, Lucas S, Lequentrec-Lalancette MF, Rouxel D, Gabalda G, Seoane L, Vu DT, Bruinsma S, Bonvalot S (2023) Airborne absolute Gravimetry with a quantum sensor, comparison with classical technologies. J Geophys Res Solid Earth 128(4):e2022JB025921. https://doi.org/10.1029/2022JB025921

Bonnefond P, Laurain O, Exertier P, Boy F, Guinle T, Picot N, Labroue S, Raynal M, Donlon C, Féménias P, Parrinello T, Dinardo S (2018) Calibrating the SAR SSH of Sentinel-3A and CryoSat-2 over the Corsica facilities. Remote Sens 10(1):92. https://doi.org/10.3390/rs10010092

Bonvalot S, Lalancette Lequentrec M-F, Bresson A, Bidel Y, Zahzam N, Bruinsma S (2018) Girafe-airgravi: Potentiel d'un gravimètre interférométrique embarqué pour la géodésie, la géophysique et l'océanographie. CNES TOSCA project n° 3673. CNES Paris

Brockmann JM, Zehentner N, Höck E, Pail R, Loth I, Mayer-Gürr T, Schuh W-D (2014) EGM_TIM_RL05: an independent geoid with centimeter accuracy purely based on the GOCE mission. Geophys Res Lett 41(22):8089–8099. https://doi.org/10.1002/2014GL061904

Brockmann JM, Schubert T, Schuh W-D (2021) An improved model of the earth's static gravity field solely derived from reprocessed GOCE data. Surv Geophys 42(2):277–316. https://doi.org/10.1007/s10712-020-09626-0

Brozena JM (1992) The Greenland Aerogeophysics project: airborne gravity, topographic and magnetic mapping of an entire continent. In: Colombo OL (ed) From mars to Greenland: charting gravity with space and airborne instruments. Springer, New York, NY, pp 203–214

Bruinsma SL, Förste C, Abrikosov O, Lemoine J-M, Marty J-C, Mulet S, Rio M-H, Bonvalot S (2014) ESA's satellite-only gravity field model via the direct approach based on all GOCE data. Geophys Res Lett 41(21):7508–7514. https://doi.org/10.1002/2014GL062045

Denker H (1998) Evaluation and Improvement of the EGG97 Quasigeoid Model for Europe by GPS and Leveling Data. Rep Finn Geod Inst 98(4):53–61

Farr TG, Rosen PA, Caro E, Crippen R, Duren R, Hensley S, Kobrick M, Paller M, Rodriguez E, Roth L, Seal D, Shaffer S, Shimada J, Umland J, Werner M, Oskin M, Burbank D, Alsdorf D (2007) The Shuttle Radar Topography Mission. Rev Geophys. https://doi.org/10.1029/2005RG000183

Forsberg R (1987) A new covariance model for inertial gravimetry and gradiometry. J Geophys Res Solid Earth 92(B2):1305–1310. https://doi.org/10.1029/JB092iB02p01305

Forsberg R, Olesen AV (2010) Airborne gravity field determination. In: Xu G (ed) Sciences of geodesy—i: advances and future directions. Springer, Berlin, Heidelberg, pp 83–104

Forsberg R, Olesen AV, Einarsson I, Manandhar N, Shreshta K (2014) Geoid of Nepal from airborne gravity survey. In: Rizos C, Willis P (eds) Earth on the edge: science for a sustainable planet. Springer, Berlin, Heidelberg, pp 521–527

Forsberg R, Olesen AV, Barnes D, Ingalls SE, Minter CF, Presicci MR (2017) Seamless geoids across coastal zones - a comparison of satellite-derived gravity to airborne gravity across the seven continents. AGU Fall Meet Abstr 2017:3–13

Forsberg R, Tscherning CC (2008) An overview manual for the GRAVSOFT Geodetic Gravity Field Modelling Programs

Forsberg R, Olesen A, Munkhtsetseg D, Amarzaya B (2007) Downward continuation and geoid determination in Mongolia from airborne and surface gravimetry and SRTM topography. In: 2007 International Forum on Strategic Technology. pp 470–475

Forsberg R (1984) A Study of Terrain Reductions, Density Anomalies and Geophysical Inversion Methods in Gravity Field Modelling. OHIO STATE UNIV COLUMBUS DEPT OF GEODETIC SCIENCE AND SURVEYING

Gatchalian RC, Forsberg R, Olesen AV (2022) A new Philippine geoid model from airborne and terrestrial gravity data. T O Terr Atmos Ocean Sci. https://doi.org/10.3319/TAO.2021.11.15.01

Green CM, Fletcher KM, Cheyney S, Dawson GJ, Campbell SJ (2019) Satellite gravity–enhancements from new satellites and new altimeter technology. Geophys Prospect 67(6):1611–9

Grigoriadis VN, Vergos GS, Barzaghi R, Carrion D, Koç Ö (2021) Collocation and FFT-based geoid estimation within the Colorado 1 cm geoid experiment. J Geod 95(5):52. https://doi.org/10.1007/s00190-021-01507-7

Haagmans R, de Min E, van Gelderen M (1993) Fast evaluation of convolution integrals on the sphere using 1-D FFT, and a comparison with existing methods for Stokes' integral. Manuscr Geod 18:227–41

Hipkin R (2000) Modelling the geoid and sea-surface topography in coastal areas. Phys Chem Earth Part Solid Earth Geod 25(1):9–16. https://doi.org/10.1016/S1464-1895(00)00003-X

Hirt C (2013) RTM gravity forward-modeling using topography/bathymetry data to improve high-degree global geopotential models in the coastal zone. Mar Geod 36(2):183–202. https://doi.org/10.1080/01490419.2013.779334

Hofmann-Wellenhof B, Moritz H (2006) Physical geodesy, 2nd edn. Springer-Verlag, Wien

Hsiao Y, Hwang C (2010) Topography-assisted downward continuation of airborne gravity: an application for geoid determination in Taiwan. TAO Terr Atmos Ocean Sci. https://doi.org/10.3319/TAO.2009.07.09.01(T)

Huang J (2017) Determining coastal mean dynamic topography by geodetic methods. Geophys Res Lett 44(21):125–11. https://doi.org/10.1002/2017GL076020

Hwang C, Guo J, Deng X, Hsu H-Y, Liu Y (2006) Coastal gravity anomalies from Retracked Geosat/GM altimetry: improvement, limitation and the role of airborne gravity data. J Geod 80(4):204–216. https://doi.org/10.1007/s00190-006-0052-x

Hwang C, Hsiao Y-S, Shih H-C, Yang M, Chen K-H, Forsberg R, Olesen AV (2007) Geodetic and geophysical results from a Taiwan airborne gravity survey: Data reduction and accuracy assessment. J Geophys Res Solid Earth. https://doi.org/10.1029/2005JB004220

Hwang C, Hsu H-J, Featherstone WE, Cheng C-C, Yang M, Huang W, Wang C-Y, Huang J-F, Chen K-H, Huang C-H, Chen H, Su W-Y (2020) New gravimetric-only and hybrid geoid models of Taiwan for height modernisation, cross-island datum connection and airborne LiDAR mapping. J Geod 94(9):83. https://doi.org/10.1007/s00190-020-01412-5

Ince ES, Barthelmes F, Reißland S, Elger K, Förste C, Flechtner F, Schuh H (2019) ICGEM—15 years of successful collection and distribution of global gravitational models, associated services, and future plans. Earth Syst Sci Data 11(2):647–674. https://doi.org/10.5194/essd-11-647-2019

Jensen TE, Olesen AV, Forsberg R, Olsson P-A, Josefsson Ö (2019) New results from Strapdown airborne Gravimetry using temperature

stabilisation. Remote Sens 11(22):2682. https://doi.org/10.3390/rs11222682

Jiang T (2018) On the contribution of airborne gravity data to gravimetric quasigeoid modelling: a case study over Mu Us area. China Geophys J Int 215(2):1308–1321. https://doi.org/10.1093/gji/ggy346

Kearsley AHW, Forsberg R, Olesen A, Bastos L, Hehl K, Meyer U, Gidskehaug A (1998) Airborne gravimetry used in precise geoid computations by ring integration. J Geod 72(10):600–605. https://doi.org/10.1007/s001900050198

Kvas A, Brockmann JM, Krauss S, Schubert T, Gruber T, Meyer U, Mayer-Gürr T, Schuh W-D, Jäggi A, Pail R (2021) GOCO06s—a satellite-only global gravity field model. Earth Syst Sci Data 13(1):99–118. https://doi.org/10.5194/essd-13-99-2021

L'Ecu F (2017) Calcul du quasi-géoïde QGF16 et de la grille de conversion altimétrique RAF16 : état d'avancement et perspectives. XYZ (n° 150):pp 49–51

Li X, Huang J, Klees R, Forsberg R, Willberg M, Slobbe DC, Hwang C, Pail R (2022) Characterization and stabilization of the downward continuation problem for airborne gravity data. J Geod 96(4):18. https://doi.org/10.1007/s00190-022-01607-y

Liebsch G, Schwabe J, Sacher M, Rülke A (2015) Unification of height reference frames in Europe. EUREF Symp 2015:31

Martinec Z (1996) Stability investigations of a discrete downward continuation problem for geoid determination in the Canadian Rocky Mountains. J Geod 70(11):805–828. https://doi.org/10.1007/BF00867158

Mayer-Gürr T, Pail R, Gruber T, Fecher T, Rexer M, Schuh W-D, Kusche J, Brockmann J-M, Rieser D, Zehentner N, Kvas A, Klinger B, Baur O, Höck E, Krauss S, Jäggi A (2015) The combined satellite gravity field model GOCO05s, Presentation at EGU general assembly 2015, Vienna, 12–17 April 2015.

McCubbine JC, Amos MJ, Tontini FC, Smith E, Winefied R, Stagpoole V, Featherstone WE (2018) The New Zealand gravimetric quasigeoid model 2017 that incorporates nationwide airborne gravimetry. J Geod 92(8):923–937. https://doi.org/10.1007/s00190-017-1103-1

Molodenskii MS (1962) Methods for study of the external gravitational field and figure of the earth. Jerus Isr Program Sci Transl 1962 Available Off Tech Serv US Dept Commer Wash

Novák P, Kern M, Schwarz KP (2001) Numerical studies on the harmonic downward continuation of band-limited airborne gravity. Stud Geophys Geod 45(4):327–345. https://doi.org/10.1023/A:1022028218964

Olesen AV, Forsberg R, Kearsley AHW (2002) Great Barrier Reef airborne gravity survey (BRAGS'99). A gravity survey piggybacked on an airborne bathymetry mission. In: Sideris MG (ed) Gravity, Geoid and Geodynamics 2000. Springer, Heidelberg, pp 247–251

Ophaug V, Breili K, Gerlach C (2015) A comparative assessment of coastal mean dynamic topography in Norway by geodetic and ocean approaches. J Geophys Res Oceans 120(12):7807–7826. https://doi.org/10.1002/2015JC011145

Pavlis NK, Holmes SA, Kenyon SC, Factor JK (2012) The development and evaluation of the earth gravitational model 2008 (EGM2008). J Geophys Res Solid Earth. https://doi.org/10.1029/2011JB008916

Poutanen M, Rózsa S (2020) The Geodesist's Handbook 2020. J Geod 94(11):109. https://doi.org/10.1007/s00190-020-01434-z

Rouxel D, Sarzeaud O, Lequentrec MF (2023) Using marine data to estimate the accuracy of free air gravity anomaly models derived from satellite altimetry. Earth Space Sci 10(5):e2022EA002672. https://doi.org/10.1029/2022EA002672

Sánchez L, Čunderlík R, Dayoub N, Mikula K, Minarechová Z, Šíma Z, Vatrt V, Vojtíšková M (2016) A conventional value for the geoid reference potential $$W_{0}$$W0. J Geod 90(9):815–835. https://doi.org/10.1007/s00190-016-0913-x

Sandwell DT, Smith WHF (1997) Marine gravity anomaly from Geosat and ERS 1 satellite altimetry. J Geophys Res Solid Earth 102(B5):10039–10054. https://doi.org/10.1029/96JB03223

Sandwell DT, Müller RD, Smith WHF, Garcia E, Francis R (2014) New global marine gravity model from CryoSat-2 and Jason-1 reveals buried tectonic structure. Science 346(6205):65–67. https://doi.org/10.1126/science.1258213

Smith DA, Holmes SA, Li X, Guillaume S, Wang YM, Bürki B, Roman DR, Damiani TM (2013) Confirming regional 1 cm differential geoid accuracy from airborne gravimetry: the Geoid Slope Validation Survey of 2011. J Geod 87(10):885–907. https://doi.org/10.1007/s00190-013-0653-0

Tozer B, Sandwell DT, Smith WHF, Olson C, Beale JR, Wessel P (2019) Global bathymetry and topography at 15 Arc sec: SRTM15 +. Earth Space Sci 6(10):1847–1864. https://doi.org/10.1029/2019EA000658

Valliant HD (1992) The Lacoste & Romberg Air/Sea Gravity Meter: An Overview. In: CRC Handbook of Geophysical Exploration at Sea, 2nd edn. CRC Press, Florida

Varga M, Pitoňák M, Novák P, Bašić T (2021) Contribution of GRAV-D airborne gravity to improvement of regional gravimetric geoid modelling in Colorado, USA. J Geod 95(5):53. https://doi.org/10.1007/s00190-021-01494-9

Verdun J, Klingelé EE, Bayer R, Cocard M, Geiger A, Kahle H-G (2003) The alpine Swiss–French airborne gravity survey. Geophys J Int 152(1):8–19. https://doi.org/10.1046/j.1365-246X.2003.01748.x

Vergos GS, Andritsanos VD, Grigoriadis VN, Pagounis V, Tziavos IN (2016) Evaluation of GOCE/GRACE GGMs Over Attica and Thessaloniki, Greece, and Wo determination for height system unification. In: Jin S, Barzaghi R (eds) IGFS 2014. Springer International Publishing, Cham, pp 101–109

Verron J, Sengenes P, Lambin J, Noubel J, Steunou N, Guillot A, Picot N, Coutin-Faye S, Sharma R, Gairola RM, Murthy DVAR, Richman JG, Griffin D, Pascual A, Rémy F, Gupta PK (2015) The SARAL/AltiKa altimetry satellite mission. Mar Geod 38(sup1):2–21. https://doi.org/10.1080/01490419.2014.1000471

Verron J, Bonnefond P, Andersen O, Ardhuin F, Bergé-Nguyen M, Bhowmick S, Blumstein D, Boy F, Brodeau L, Crétaux J-F, Dabat ML, Dibarboure G, Fleury S, Garnier F, Gourdeau L, Marks K, Queruel N, Sandwell D, Smith WHF, Zaron ED (2021) The SARAL/AltiKa mission: a step forward to the future of altimetry. Adv Space Res 68(2):808–828. https://doi.org/10.1016/j.asr.2020.01.030

Vu DT, Bruinsma S, Bonvalot S (2019) A high-resolution gravimetric quasigeoid model for Vietnam. Earth Planets Space 71(1):65. https://doi.org/10.1186/s40623-019-1045-3

Vu DT, Bruinsma S, Bonvalot S, Remy D, Vergos GS (2020) A Quasigeoid-derived transformation model accounting for land subsidence in the Mekong delta towards height system unification in Vietnam. Remote Sens 12(5):817. https://doi.org/10.3390/rs12050817

Vu DT, Bonvalot S, Bruinsma S, Bui LK (2021a) A local lithospheric structure model for Vietnam derived from a high-resolution gravimetric geoid. Earth Planets Space 73(1):92. https://doi.org/10.1186/s40623-021-01415-2

Vu DT, Bruinsma S, Bonvalot S, Bui LK, Balmino G (2021b) Determination of the geopotential value on the permanent GNSS stations in Vietnam based on the geodetic boundary value problem approach. Geophys J Int 226(2):1206–1219. https://doi.org/10.1093/gji/ggab166

Vu DT, Verdun J, Cali J, Maia M, Poitou C, Ammann J, Roussel C, D'Eu J-F, Bouhier M-É (2024) High-resolution gravity measurements on board an autonomous underwater vehicle: data reduction and accuracy assessment. Remote Sens 16(3):461. https://doi.org/10.3390/rs16030461

Wang YM, Sánchez L, Ågren J, Huang J, Forsberg R, Abd-Elmotaal HA, Ahlgren K, Barzaghi R, Bašić T, Carrion D, Claessens S, Erol B, Erol S, Filmer M, Grigoriadis VN, Isik MS, Jiang T, Koç Ö, Krcmaric J, Li X, Liu Q, Matsuo K, Natsiopoulos DA, Novák P, Pail R, Pitoňák M, Schmidt M, Varga M, Vergos GS, Véronneau M, Willberg M, Zingerle P (2021) Colorado geoid computation experiment: overview and summary. J Geod 95(12):127. https://doi.org/10.1007/s00190-021-01567-9

Wessel P, Watts AB (1988) On the accuracy of marine gravity measurements. J Geophys Res Solid Earth 93(B1):393–413. https://doi.org/10.1029/JB093iB01p00393

Wessel P, Luis JF, Uieda L, Scharroo R, Wobbe F, Smith WHF, Tian D (2019) The generic mapping tools version 6. Geochem Geophys Geosystems 20(11):5556–5564. https://doi.org/10.1029/2019GC008515

Wong L, Gore R (1969) Accuracy of geoid heights from modified stokes kernels. Geophys J R Astron Soc 18(1):81–91. https://doi.org/10.1111/j.1365-246X.1969.tb00264.x

Wu Y, Abulaitijiang A, Featherstone WE, McCubbine JC, Andersen OB (2019) Coastal gravity field refinement by combining airborne and ground-based data. J Geod 93(12):2569–2584. https://doi.org/10.1007/s00190-019-01320-3

Zhao Q, Strykowski G, Li J, Pan X, Xu X (2017) Evaluation and comparison of the processing methods of airborne gravimetry concerning the errors effects on downward continuation results: case studies in Louisiana (USA) and the Tibetan Plateau (China). Sensors 17(6):1205. https://doi.org/10.3390/s17061205

Zhao Q, Xu X, Forsberg R, Strykowski G (2018) Improvement of downward continuation values of airborne gravity data in Taiwan. Remote Sens 10(12):1951. https://doi.org/10.3390/rs10121951